ACS APPLIED MATERIALS & INTERFACES

www.acsami.org

Research Article

Ultrafine Sodium Sulfide Clusters Confined in Carbon Nanopolyhedrons as High-Efficiency Presodiation Reagents for Sodium-Ion Batteries

Xiaoxiao Liu, Yuchen Tan, Wenyu Wang, Peng Wei, Zhi Wei Seh, and Yongming Sun*

Cite This: *ACS Appl. Mater. Interfaces* 2021, 13, 27057−27065

Read Online

ACCESS | Metrics & More | Article Recommendations | Supporting Information

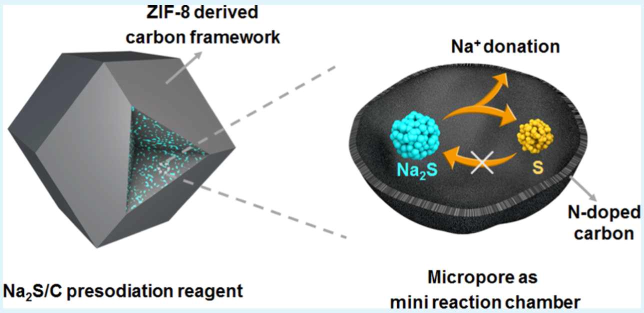

ABSTRACT: Sodium loss at the anode in the initial sodiation process significantly reduces the energy density of sodium-ion batteries (SIBs). Here, a high-capacity Na_2S/C nanocomposite featuring ultrafine Na_2S nanoclusters (<2 nm) confined in ZIF-8-derived microporous N-doped carbon is fabricated and employed as a cathode presodiation reagent to compensate for this sodium loss and increase the energy density of SIBs. The ultrafine size of Na_2S enables fast reaction kinetics for sodium extraction and the carbon matrix provides good electronic conductivity. Also, the overall particle size of the Na_2S/C nanocomposite (∼40 nm) is close to that of conductive additive. The above features enable it to replace a partial amount of conductive additive and compensate for the sodium loss at the anode concurrently. As a demonstration, the $Na_3V_2(PO_4)_3$ electrode with 5 wt % Na_2S/C and 5 wt % carbon black was fabricated, and it displayed a 19 mAh g^{-1} higher initial charge specific capacity than that of the counterpart with 10% carbon black without the addition of Na_2S/C, realizing an increased energy density from 178 to 263 Wh kg^{-1} in the full cell configuration pairing with a hard carbon anode. Moreover, a stable cycling performance up to 200 cycles with an average capacity loss of 0.024 mAh g^{-1} per cycle was achieved for the presodiated $Na_3V_2(PO_4)_3$ electrode.

KEYWORDS: *Na_2S, cathode presodiation, space confinement, microporous carbon, sodium-ion batteries*

1. INTRODUCTION

Sodium-ion batteries (SIBs) have attracted intensive attention recently due to the abundance of sodium resources in nature, considerably high energy density, and low cost, making them an alternative to the widely used lithium-ion batteries (LIBs) in certain applications, such as large-scale energy storage systems.[1−5] In the state-of-the-art SIBs, the cathode material is the only source of electrochemically active sodium. During the initial battery cycle, side reactions take place at the anode−electrolyte interphase and a solid electrolyte interphase (SEI) is formed on the surface, which consumes active sodium from the cathode.[6−8] This sodium loss due to SEI formation at the anode significantly reduces the energy density of SIBs and hinders the development of high-energy-density SIBs. Thus, it is highly desired to find an effective approach to address the active sodium loss and improve the energy density of SIBs.

Presodiation is regarded as a promising strategy to compensate for the initial sodium loss by introducing an extra electrochemically active sodium source into the battery.[9] Till now, several presodiation techniques/approaches have been developed. Electrochemical presodiation of anodes using metallic sodium as the counter electrode in an assembled battery and applying an external potential or direct contact between the sodium metal and the working electrode has shown its effectiveness in compensating the sodium loss and increasing the initial Coulombic efficiency (ICE) of various anodes.[10] However, such an approach involves the disassembly and reassembly of battery, which is tedious and costly, and thus unsuitable for large-scale application. Owing to the high specific capacity of sodium metal (1165 mAh g^{-1}), sodium powders were proposed as effective presodiation reagents for anodes.[11] Owing to the prestored sodium on the anodes, the ICE of hard carbon anode was increased and a remarkable enhancement of energy density at full cell level was realized. Despite the advantage of high capacity and presodiation efficiency of sodium metal, its high reactivity leads to serious safety concerns, making sodium metal powders incompatible with battery manufacturing. In our previous work, we conducted a facile solution chemical route using sodium naphthaline (Naph-Na) as the presodiation reagent to preform

Received: March 18, 2021
Accepted: May 24, 2021
Published: June 3, 2021

https://doi.org/10.1021/acsami.1c05144
ACS Appl. Mater. Interfaces 2021, 13, 27057−27065

a SEI layer on a carbon anode, which significantly improved the energy density of SIBs at full cell level.[12] An irreversible capacity of 60 mAh g^{-1} was replenished for the carbon anode, and the energy density of a $Na_{0.9}[Cu_{0.22}Fe_{0.30}Mn_{0.48}]O_2$||carbon full cell was increased from 141 to 240 Wh kg^{-1} using the presodiated carbon anode. To promote the fast application of presodiation in the battery industry, it is highly desirable to explore more practical approaches for high-efficiency presodiation.

Cathode presodiation reagents are compatible with current battery manufacturing since no other complicated operations and harsh conditions need to be involved. Sodium salts, such as $NaCrO_4$,[13] $Na_2C_4O_4$,[14] $Na_2C_2O_4$,[15] DTPA-5Na,[16] and NaN_3,[17,1817,18] have been investigated as cathode presodiation additives to solve the current irreversible capacity issues of anodes in SIBs. Sodium ions can be extracted during the first charging process for these agents to compensate for the sodium loss at the anode. However, undesirable gases (N_2 and/or CO_2) are generated concomitantly, which are detrimental to the cycle life and safety of batteries. In addition, another drawback of these materials is the limited donable sodium-ion capacity (often less than 400 mAh g^{-1}), which cannot fulfill the high energy density requirement of SIBs. Furthermore, after the sacrifice of these materials, vacancies or voids would be produced in electrodes, which may pose a threat to the cycling stability of batteries. Therefore, addressing the above-mentioned issues and developing a promising cathode presodiation additive are still real challenges. Sodium sulfide (Na_2S) has gained much attention as a cathode for sodium−sulfur batteries in recent years by virtue of its high theoretical specific capacity (687 mAh g^{-1}, ca. 6 times higher than ∼110 mAh g^{-1} for the typical insertion compound $Na_3V_2(PO_4)_3$ cathode).[19−22] However, one serious problem for Na_2S cathode is the low energy efficiency of the battery resulting from the large voltage polarization between charge and discharge. A high activation voltage of 3.5 V or above is necessary to fully convert Na_2S to S, while the sodiation voltage of S is usually lower than 2 V.[23−25] Although it is a critical drawback for the Na_2S cathode used for sodium−sulfur battery, it meets the basic requirement as a cathode presodiation material for SIBs. As a cathode additive, a high sodium-ion capacity can be extracted from Na_2S during the charging process of the cathode with a cutoff voltage higher than 4 V in SIBs, and its charge product (S) would not be sodiated during the following discharge process with a cutoff voltage higher than 2.5 V of SIBs. Thus, it can contribute to a high donable sodium-ion capacity. However, before its application, several hindrances need to be solved,[26−30] which include the electronically and ionically insulating nature of the Na_2S material and the conversion product S and dissolution of long-chain polysulfides into the electrolyte that triggers side reactions and large volume variation (∼160%) during the conversion of Na_2S to S.

Herein, we report a well-crafted Na_2S/C nanocomposite in which ultrafine Na_2S nanoclusters are confined in the micropores of N-doped carbon nanoparticles (∼40 nm) derived from zeolitic imidazolate framework material (ZIF-8). The ultrafine Na_2S nanoclusters maintain close contact with conductive carbon, which ensures fast Na^+ and electron transport and facilitates the Na−S electrochemical conversion reactions. Moreover, the ultrasmall size of Na_2S nanoclusters shortens the ion-diffusion pathway and thus improves the reaction kinetics and increases the utilization of the active material. Due to the ultrafine size and confinement effect of micropores, the intermediate polysulfides would not diffuse to the electrolyte. Since Na_2S is already in the fully expanded form and well confined in the limited space, it can also alleviate the volume change issue during sodium donation. Specifically, the Na_2S/C nanocomposite shows particle size similar to that of the conducting additive in electrode and good electronic conductivity. Both features provide an opportunity for it to replace the partial amount of the conductive additive. With such a delicate design, the fabricated Na_2S/C composite displayed an initial donable charge capacity of 553 mAh g^{-1}. When employed as a cathode presodiation additive, the presodiated $Na_3V_2(PO_4)_3$ electrode with 5% addition of Na_2S/C and 5% carbon black demonstrated a higher first-cycle charge capacity of 128 mAh g^{-1}, compared to 109 mAh g^{-1} for the pristine $Na_3V_2(PO_4)_3$ electrode with 10% carbon black without the addition of Na_2S/C. Meanwhile, the $Na_3V_2(PO_4)_3$ electrode with such a presodiation additive also demonstrated a long service life of up to 200 cycles with a negligible capacity decay. The results obtained in this work can shed light on the design of high-energy-density sodium-ion full batteries using a high-capacity anode material with low ICE.

2. EXPERIMENTAL SECTION

2.1. Materials. Commercially available reagents of 2-methylimidazole, zinc nitrate hexahydrate, methanol, sulfur powders, dimethoxyethane (DME), and naphthalene (Naph) were used as received without further purification. $Na_3V_2(PO_4)_3$ materials were purchased from Hubei Energy Technology Co., Ltd. Carbon anode materials were purchased from Guangdong Canrd New Energy Technology Co., Ltd.

2.2. Synthesis of Zn-Based ZIF-8 Nanocrystals. 2-Methylimidazole (Sigma) of 1621.2 mg and zinc nitrate hexahydrate ($Zn(NO_3)_2 \cdot 6H_2O$, Acros) of 1468.8 mg were dissolved in 100 mL of methanol (Sinopharm) solvent. The methanol solution of 2-methylimidazole was poured into the $Zn(NO_3)_2 \cdot 6H_2O$ solution with vigorous stirring, resulting in the formation of milky suspension. After stirring for another 1 min, the mixed solution was sealed with a plastic film and left for 12 h at ambient temperature. The produced white particles were washed with methanol three times and dried under a vacuum at room temperature.

2.3. Synthesis of Na_2S/C Presodiation Additives. First, the N-doped microporous carbon was obtained by pyrolyzing the as-prepared Zn-based ZIF-8 nanocrystals at 700 °C for 1 h in a N_2 atmosphere. The remaining zinc residuals in the microporous carbon framework were removed by washing with a 5 wt % HCl solution. Then, the N-doped microporous carbon/sulfur nanocomposite was constructed using a simple melt-diffusion method in which sulfur and N-doped microporous carbon were mixed in a weight ratio of 7:3 and sealed in an Ar-filled stainless steel reactor and treated at 155 °C for 12 h. The residual sulfur on the carbon surface was removed by treating the C/S composite at 280 °C in Ar for 1 h, creating a conductive surface. Finally, the Na_2S/C composite was achieved after the reaction between the C/S nanocomposite and 0.2 M Naph-Na/DME solution with a S:Na mole ratio of 1:2 in an Ar atmosphere at room temperature.

2.4. Material Characterization. Scanning electron microscopy (SEM) equipped with an energy-dispersive spectrometer (Gemini-SEM300) was used to characterize the morphology and elemental distribution of the as-prepared materials and the electrodes before and after cycles. The cycled electrode was washed with diethyl carbonate (DEC) before characterizations. Transmission electron microscopy (TEM) images and high-angle annular dark-field scanning TEM (HAADF-STEM) images as well as the corresponding elemental distribution mappings were collected on a Talos F200X instrument. Nitrogen adsorption/desorption isotherms were obtained on an ASAP 2460 apparatus (Micromeritics). The sulfur content in the N-

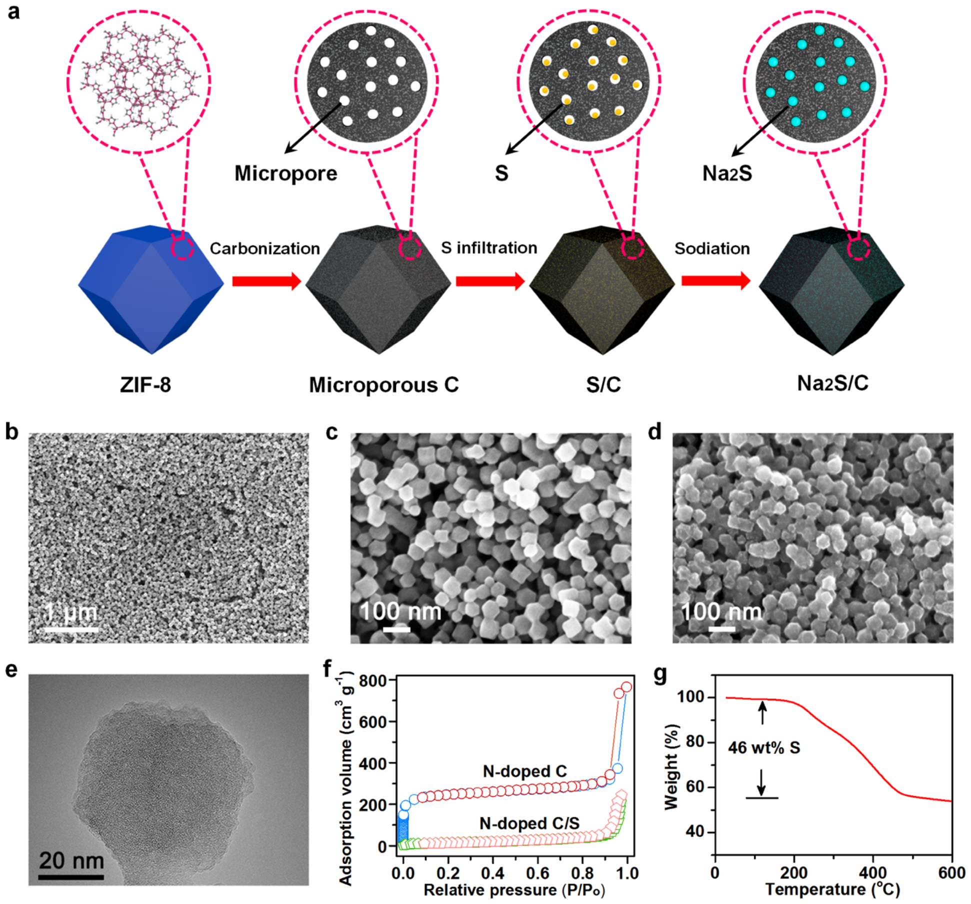

Figure 1. (a) Schematic illustration of the preparation process for the Na_2S/C nanocomposite. (b, c) SEM images of ZIF-8 nanocrystals. (d) SEM and (e) TEM images of the ZIF-8-derived N-doped carbon (N-doped C). (f) Nitrogen adsorption/desorption isotherms of the as-prepared N-doped C with and without sulfur injection. (g) TG curves for N-doped C/S nanocomposites.

doped microporous carbon was detected using a thermogravimetric (TG) analysis apparatus in an argon atmosphere. The valence state and composition of the as-prepared materials were detected by X-ray photoelectron spectroscopy (Thermo VG Scientific) with a monochromatic Al *Kα* X-ray source. The X-ray diffraction (XRD) pattern of the as-prepared materials was recorded on a PANalytical B.V. instrument (Empyrean) with Cu $K\alpha_1$ radiation.

2.5. Electrochemical Measurements. The $Na_3V_2(PO_4)_3$ electrode was fabricated by casting the slurry containing 80 wt % commercial active material, 10 wt % carbon black, and 10 wt % poly(vinylidene fluoride) binder (PVDF) in *N*-methyl-2-pyrrolidinon solvent onto an aluminum foil and then drying at 80 °C for 6 h under a vacuum. The fabrication of the presodiated $Na_3V_2(PO_4)_3$ electrode was similar to that of the pristine $Na_3V_2(PO_4)_3$ electrode except that 5 wt % carbon black was substituted by the as-synthesized Na_2S/C nanocomposite. The negative electrode using copper foil as the current collector consisted of 90 wt % hard carbon, 5 wt % carbon black, and 5 wt % PVDF. Coin cells were assembled in a glove box filled with high-purity argon with the content of both H_2O and O_2 less than 0.1 ppm. Glass fibers (Whatman) were employed as separators. One molar $NaClO_4$ in ethylene carbonate (EC) and diethylene carbonate (DEC) with the addition of 5 vol % fluoroethylene carbonate (FEC) was used as the electrolyte. The voltage−capacity profiles and the service life of the as-prepared materials were carried out on a multichannel battery testing instrument (Neware, China) in the potential range of 2.5−4.0 V using sodium metal as the counter electrode in half-cell configurations. The $Na_3V_2(PO_4)_3$||hard carbon full cell was cycled at a current density of 0.1C in the potential range of 1.0−3.9 V with the capacity ratio of anode to cathode of ca. 1.16. The energy density of the $Na_3V_2(PO_4)_3$||hard carbon full cell with and without presodiation is calculated based on the mass loading of the $Na_3V_2(PO_4)_3$ active material.

3. RESULTS AND DISCUSSION

Figure 1a schematically illustrates the preparation process for the Na_2S/C nanocomposites. Zn-based microporous ZIF-8 nanocrystals were first synthesized according to the previous report by mixing zinc nitrate hydrate with 2-methylimidazole in the methanol solution.[31] Then, after carbonization and washing with dilute HCl, ZIF-8 precursors were converted into the highly conductive nitrogen-doped microporous carbon (N-doped C). The Na_2S/C nanocomposites were finally obtained by infusing molten sulfur into the microporous carbon, followed by the sodiation of sulfur to Na_2S through a simple chemical solution reaction. The detailed synthesis procedures of ZIF-8, nitrogen-doped microporous carbon, and Na_2S/C are described in Section 2. Scanning electron microscopy (SEM) and transmission electron microscopy (TEM) equipped with energy-dispersive X-ray (EDX) mapping were used to investigate the morphology, structure, composition, and distribution of the products. As shown in Figure 1b,c, the as-prepared ZIF-8 nanocrystals exhibit a polyhedron-like morphology with an average particle size of ca. 60 nm. After carbonization, the size of the nitrogen-doped microporous carbon shrank into a smaller value of ca. 40 nm, while their polyhedron-like morphology was well preserved by virtue of the robust framework of ZIF-8 crystals during the high-temperature carbonization procedure (Figures 1d and S1,

https://doi.org/10.1021/acsami.1c05144
ACS Appl. Mater. Interfaces 2021, 13, 27057−27065

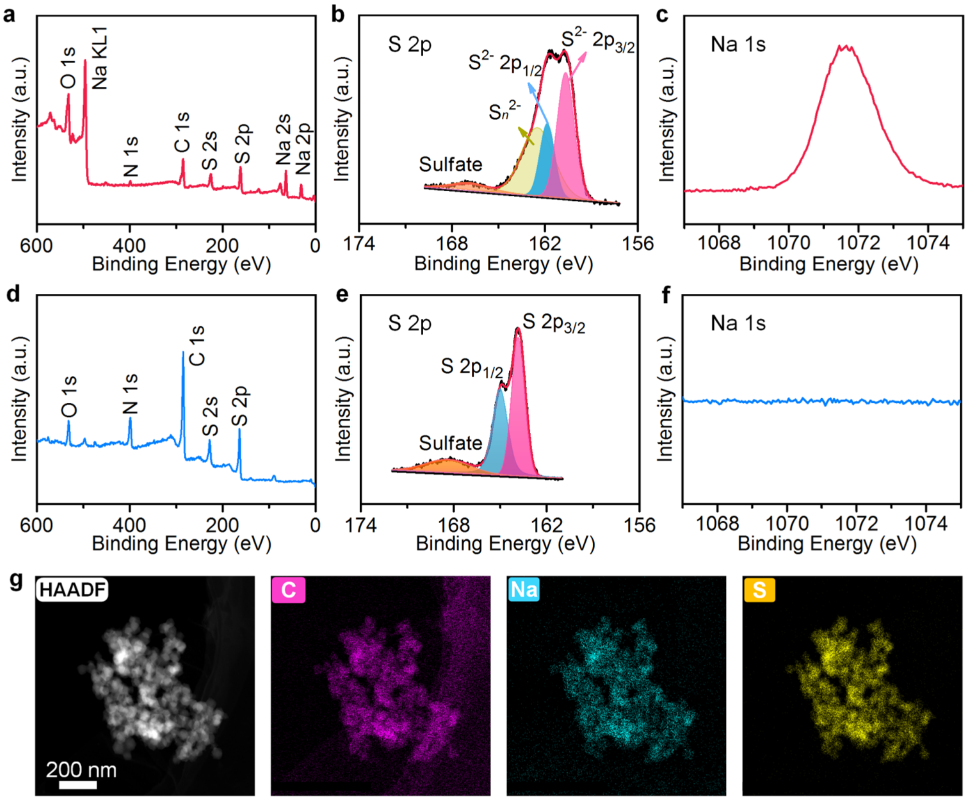

Figure 2. (a) Survey XPS spectrum and high-resolution (b) S 2p and (c) Na 1s XPS spectra for the Na_2S/C nanocomposite. (d) Survey XPS spectrum and high-resolution (e) S 2p and (f) Na 1s XPS spectra for the S/C nanocomposite. (g) HAADF image and the corresponding elemental mapping images of C, Na, and S for the Na_2S/C nanocomposite.

Supporting Information). As revealed by the high-resolution TEM image (Figure 1e), the obtained carbon matrix was amorphous since a relatively low carbonization temperature was used to reduce nitrogen loss for the N-doped carbon. The corresponding elemental mapping results revealed that the as-prepared ZIF-8 derived carbon framework was homogeneously doped with nitrogen (Figure S1), which has been proven as efficient and active adsorption sites for polysulfides to inhibit their dissolution into the electrolyte.[32−34] As demonstrated by the nitrogen adsorption/desorption isotherm, the as-synthesized N-doped carbon displayed a type I isotherm with sharp uptakes at relative pressures (P/P_0) of less than 0.05 (Figure 1f), suggesting the microporous structure of carbon.[35] In light of the abundant micropores, a high (Brunauer, Emmett, and Teller, BET) surface area of 747 $m^2\ g^{-1}$ was obtained, which was beneficial for sulfur loading. The pore size was mainly concentrated at less than 2 nm based on the nitrogen adsorption/desorption isotherm characterization. In comparison, the (BET) surface area of the S/C nanocomposite decreased to 51 $m^2\ g^{-1}$, suggesting the successful infiltration of sulfur into micropores of the N-doped carbon. X-ray diffraction (XRD) pattern showed weak peaks assigned to S_8 (Figure S2), suggesting that most of the sulfur was confined in the micropores of N-doped carbon. The result of thermogravimetric analysis (TGA) indicates that the S content in the C/S composite is 46 wt % (Figure 1g), ca. 10 wt % from the outside surface and ca. 36 wt % from the micropores of the carbon.[36] High-angle annular dark-field scanning transmission electron microscopy (HAADF-STEM) and the corresponding elemental mapping images further revealed that sulfur was homogeneously dispersed in the microporous carbon matrix (Figure S3).

According to the above analysis, we successfully loaded sulfur into the micropores of the ZIF-8-derived N-doped carbon. The chemical conversion of S into Na_2S takes place within the microreactor of these micropores of the carbon, and the sizes of the S and Na_2S particles are confined by these micropores, producing a Na_2S/C composite structure with ultrafine Na_2S nanocluster (<2 nm) embedded in a N-doped carbon matrix. X-ray photoelectron spectroscopy (XPS) and transmission electron microscopy (TEM) equipped with EDX are employed to characterize the elemental valance state and composition change of the S/C composites after a chemical sodiation reaction. Due to the lower redox chemical potential of Naph-Na than that of sulfur, the latter can be easily converted into Na_2S with naphthalene as a reaction catalyst carrier.[12,37−39] As revealed in Figure 2a,d, signals assigned to elemental Na appear and signals ascribed to elemental C and N remain in the full spectrum of the composite after chemical sodiation, indicating the successful introduction of Na element into the composite without destroying its original composition. As demonstrated by the high-resolution S 2p XPS results (Figure 2b,e), the peak positions for S 2p shift to positions with lower binding energy (from 165.0 eV for S $2p_{1/2}$ and 163.8 eV for S $2p_{3/2}$ to 161.7 eV for S^{2-} $2p_{1/2}$ and 160.6 eV for S^{2-} $2p_{3/2}$) after chemical sodiation,[40,41] validating the conversion of elemental sulfur to S^{2-} in Na_2S.[20,42,43] The appearance of Na^+ signal in the high-resolution Na 1s XPS spectra also supports the formation of Na_2S after the chemical sodiation reaction (Figure 2c,f). A weak peak located at 162.4 eV was observed, attributed to the S_n^{2-} of intermediate polysulfides,[43,44] which indicated the incomplete transformation of S to Na_2S. Benefiting from the space confinement effect, the intermediate polysulfides can be suppressed from dissolving into the electrolyte during the electrochemical reaction process.[32,45]

As shown in Figure S4, no bulk particles are observed in the TEM images of the Na_2S/C nanocomposite, indicating that the as-formed Na_2S particles are well confined in micropores of the N-doped carbon. No diffraction peaks were observed in the XRD pattern of the Na_2S/C nanocomposite, suggesting the ultrafine size of Na_2S (Figure S5). Confined by the micropores of the carbon matrix, the size of the Na_2S clusters was less than 2 nm. HAADF and the corresponding elemental distribution mapping images showed a uniform distribution of Na and S in the carbon matrix (Figure 2g), further suggesting that Na_2S was homogeneously dispersed in the N-doped carbon matrix. Therefore, a cathode presodiation reagent with ultrafine Na_2S clusters confined in ZIF-8-derived N-doped microporous carbon was successfully synthesized. Benefiting from the limited-domain features of Na_2S in micropores of N-doped C, the problems of low conductivity and dissolution of polysulfide intermediates, as well as the volume change during conversion reaction of Na_2S, can be well mitigated. Thus, it can be expected that the Na_2S/C nanocomposite can afford a high donable sodium-ion capacity when used as a prosodiation additive and improve the energy density of a full cell.

Na_2S has been widely investigated as an attractive cathode material for sodium-ion batteries by virtue of its high specific capacity and sodium-containing features that can be coupled with a sodium-free anode to avoid the safety problems of the sodium-metal anode.[19,46] During the charging process, the Na_2S electrode donates electrochemically active Na and converts to S ($Na_2S \rightarrow 2Na^+ + 2e^- + S$) in a suitable cutoff charge voltage above 3.5 V (e.g., 4.0 V, Figure 3a). During the discharge process with the cutoff discharge voltage above 2 V (e.g., 2.5 V), the S remains stable and would not transform to Na_2S due to the remarkable voltage hysteresis of the S cathode for sodiation.[41] The onset potential of S conversion to Na_2S is usually less than 2 V, which is lower than the cutoff voltage for most of the cathode materials for SIBs, such as $Na_{0.9}[Cu_{0.22}Fe_{0.30}Mn_{0.48}]O_2$, $Na_3V_2(PO_4)_3$, and $NaFeO_2$, etc.[12,21,47] Thus, the features of high sodium donation efficiency and low sodium intake voltage make Na_2S an ideal cathode presodiation reagent.

As shown in Figure 3b, we first investigated the donable sodium-ion capacity of the as-synthesized Na_2S/C composite in a half-cell using sodium metal as the counter electrode at a current density of 20 mA g^{-1}. The as-prepared Na_2S/C composite converted into a S/C composite during the initial charge process and delivered a charge specific capacity of 553 mAh g^{-1} (based on the mass of Na_2S), which correlated to 81% of the theoretical value for Na_2S (687 mAh g^{-1}) and ca. 5 times higher than the specific capacity of the $Na_3V_2(PO_4)_3$ cathode. Such a high donable sodium-ion capacity of Na_2S/C can be ascribed to the synergistic effects consisting of the high electronic conductivity of carbon framework that ensures fast electron transport, ultrafine size of Na_2S nanocluster that enables fast reaction kinetics, and nanoscale space confinement effect of the micropores that inhibits polysulfide dissolution.[45] Due to the high cutoff discharge voltage (2.5 V) for the S/C cathode, S would not convert into Na_2S reversibly in the discharge process, leading to a negligible discharge capacity. Therefore, when applying Na_2S/C as a cathode presodiation additive, abundant electrochemically active sodium ions can be supplied to compensate for the sodium loss at anodes. The electrochemically formed S after the extraction of sodium was well encapsulated in the micropores and maintained intimate contact with the highly conductive carbon matrix, as verified by the HAADF and the corresponding elemental mapping images of the products shown in Figure S6. To show the effect of sodium compensation of the Na_2S/C composite on the cathode, we fabricated a $Na_3V_2(PO_4)_3$ electrode with 5 wt % Na_2S/C presodiation additive, 5 wt % carbon black, 10 wt % binder, and 80 wt % active material and investigated its electrochemical performance. As a control, we also prepared the $Na_3V_2(PO_4)_3$ electrode with 10 wt % carbon black, 10 wt % binder, and 80 wt % active materials. The detailed information about the electrode and battery fabrication is elaborated in Section 2. Figure 3c shows the first-cycle voltage−capacity curves of the $Na_3V_2(PO_4)_3$ cathode with and without Na_2S/C presodiation additives. Due to the high donable sodium-ion capacity of the Na_2S/C composite, the $Na_3V_2(PO_4)_3$ cathode with 5 wt % presodiation additive delivered a higher specific capacity of 128 mAh g^{-1} than that of 109 mAh g^{-1} for the counterpart without the addition of the Na_2S/C composite. The excess specific sodium-ion capacity of 19 mAh g^{-1} can compensate for the sodium loss at the anode and increase the reversible electrochemically active Na^+ in a full cell and thus improve the energy density of batteries

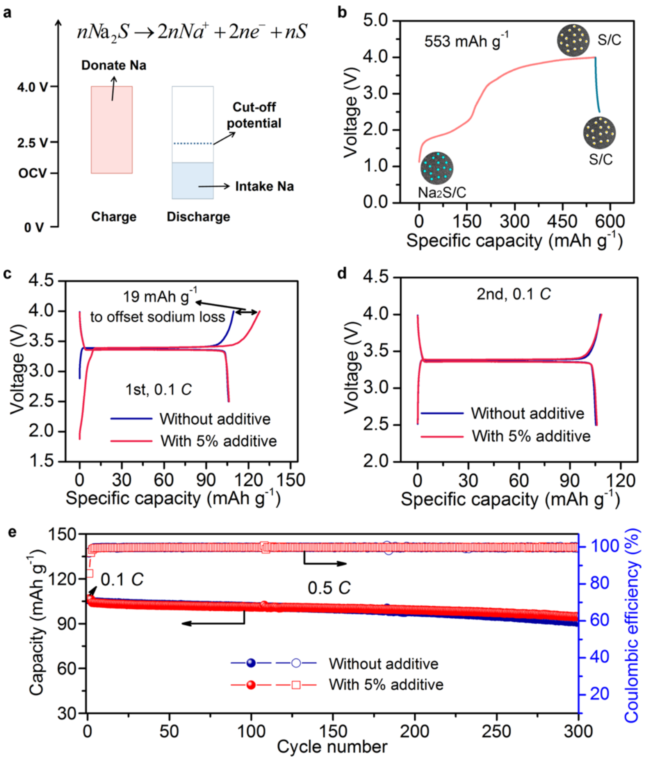

Figure 3. (a) Schematic illustration of the sodium extraction and intake potential for Na_2S/C nanocomposite. The electrochemical sodium extraction process for Na_2S is also illustrated. (b) First cycle voltage−capacity curve of the Na_2S/C presodiation composite with the cutoff voltage between 2.5 and 4.0 V. Insets show the corresponding evolution of the Na_2S/C nanocomposite. Comparison of (c) the first-cycle and (d) the second-cycle voltage−capacity profiles for the $Na_3V_2(PO_4)_3$ electrode with and without the Na_2S/C additive. (e) Cycling performance of the $Na_3V_2(PO_4)_3$ electrode with and without the Na_2S/C additive.

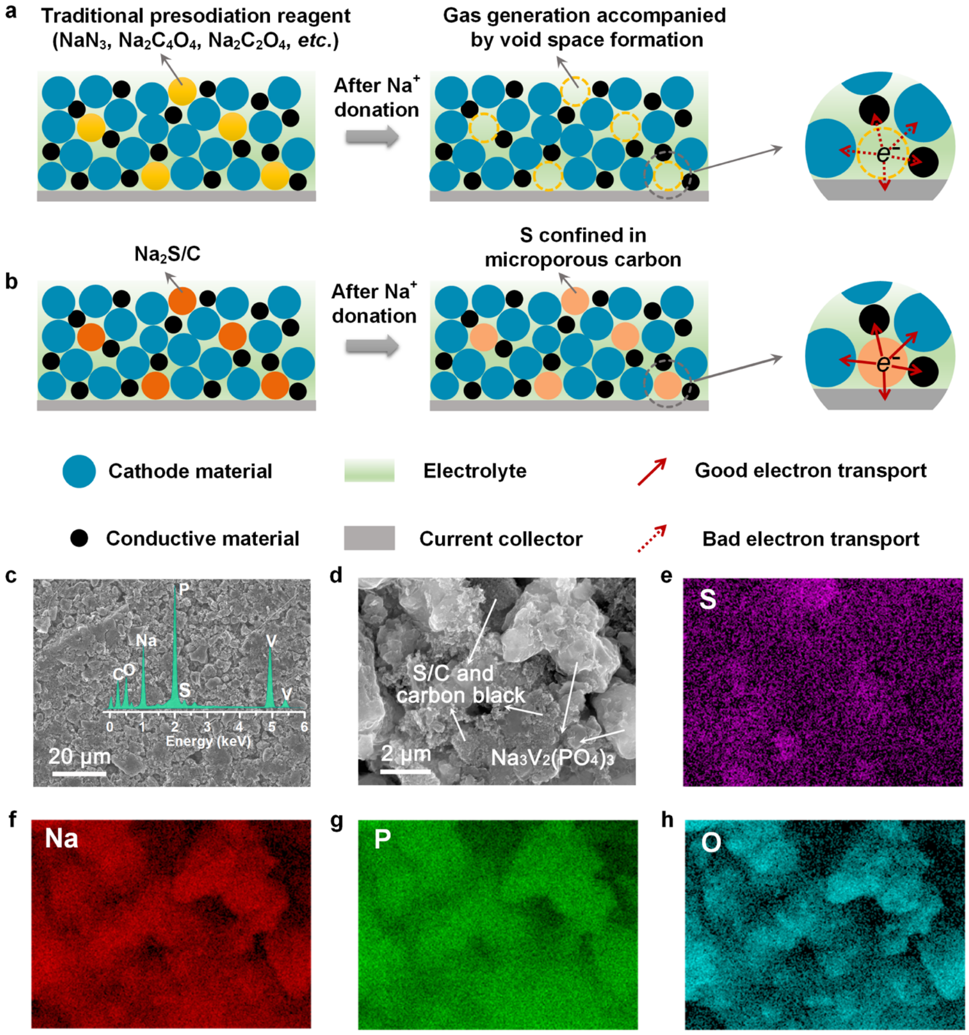

Figure 4. Schematic illustration of the evolution for (a) the traditional cathode presodiation additives and (b) the as-synthesized Na_2S/C cathode presodiation additive in the electrode during the electrochemical process. (c−h) SEM and the corresponding elemental mapping images of the $Na_3V_2(PO_4)_3$ electrode with presodiation additive after cycles. Inset in (c) is the EDX spectrum of the $Na_3V_2(PO_4)_3$ electrode with presodiation additive after 100 cycles.

(Figure S7). As a result, the energy density of the $Na_3V_2(PO_4)_3$||C full cell increased from 178 to 263 Wh kg^{-1} with the addition of 5 wt % Na_2S/C at the cathode side. The discharge profiles of the $Na_3V_2(PO_4)_3$ cathode with and without the presodiation additive coincide well with each other, indicating that the presodiation additive poses no negative effect on the discharge properties of the $Na_3V_2(PO_4)_3$ cathode materials. The second-cycle voltage−capacity profiles of the $Na_3V_2(PO_4)_3$ cathode with and without the Na_2S/C composite overlap well (Figure 3d), suggesting that the sodium donation process of the Na_2S/C composite only occurred in the first-cycle charge process and had no effect on the specific capacity of $Na_3V_2(PO_4)_3$ cathode in the subsequent cycles, which was of key importance for cathode presodiation additives. As shown in Figure 3e, the $Na_3V_2(PO_4)_3$ electrodes with and without the Na_2S/C composite demonstrate comparable cycling stability. Both electrodes exhibited stable cycling for 300 cycles without an obvious capacity degradation, with the Coulombic efficiency close to 100%, further indicating the stability of the S/C nanocomposite after the donation of active sodium in the electrode and excellent robustness of the presodiated electrode. Electrochemical impedance spectroscopy (EIS) of the $Na_3V_2(PO_4)_3$ (NVPO) electrodes with and without the Na_2S/C additive after different cycles are shown in Figure S8. Both $Na_3V_2(PO_4)_3$ electrodes displayed similar impedance before cycling. After 50 cycles, the $Na_3V_2(PO_4)_3$ electrode with the Na_2S/C additive demonstrated lower overall impedance than the pristine $Na_3V_2(PO_4)_3$ electrode, indicating that the *in situ* electrochemical formed S/C did not pose negative effects on the conductivity of electrodes. Therefore, by simply replacing the partial amount of conductive additive with the Na_2S/C composite in the cathode, high prosodiation efficiency is realized for the cathode, which is promising for improving the energy density of full SIBs.

An ideal cathode presodiation reagent should meet several important criteria, including high donable sodium-ion capacity, no/negligible negative effects on capacity and cycling of the cathode, good compatibility with the existing battery manufacturing process, and no detrimental gas generation. When traditional cathode presodiation additives such as NaN_3, $Na_2C_4O_4$, and $Na_2C_2O_4$, etc. are applied in the cathodes, undesirable gases are generated accompanied by the formation of void space during the sodium donation process (Figure 4a). The unrecoverable void space in the electrode may destroy the integrated construction of the electrode and cut off the transport pathways of electrons from particle to particle and particle to current collector, leading to inferior electron transport at the electrode level. Furthermore, the shrinkage of the presodiation additives after the extraction of active sodium can cause strain and stress and induce cracks in the electrode with some adhesion failure, resulting in the detachment of active materials from the current collector and accelerating battery failure. The proposed and well-designed Na_2S/C cathode presodiation material can offset the drawbacks of the above-mentioned cathode presodiation materials. Na_2S converts to S during the sodium donation process without generating detrimental gases (Figure 4b). Since Na_2S is well confined in the micropores of the carbon framework, the micropores can serve as mini-electrochemical reaction chambers restricting the diffusion of Na_2S_n species into the electrolytes during the conversion between Na_2S and S.[48] The electrochemically formed insulating S is confined in the micropores of conductive carbon framework and the overall volume does not change before and after the extraction of active sodium, thus high conductivity of the additive is maintained. In our experiment, we replaced the 5 wt % conductive carbon with the Na_2S/C nanocomposite. Thus, the residual S/C nanocomposite after the sodium donation can work as a conductive additive and afford excellent electron accessibility among the active materials (Figure 4b), making the well-designed Na_2S/C an ideal cathode presodiation material. Figure 4c−h shows the SEM images of the $Na_3V_2(PO_4)_3$ electrode with Na_2S/C presodiation additive after cycling. No obvious cracks were observed in the electrode compared to the electrode before cycling, which is similar to the situation of the bare $Na_3V_2(PO_4)_3$ electrode (Figures S9 and S10), again supporting the the fact that the elaborately synthesized Na_2S/C cathode presodiation material has no negative influence on the structural stability of the electrode. The robust structural stability of the conductive S/C composite in the electrode leads to a comparatively stable cycle life of the $Na_3V_2(PO_4)_3$ cathode with the addition of the Na_2S/C nanocomposite that of the pristine $Na_3V_2(PO_4)_3$ cathode. The EDX result reveals (inset in Figure 4c) that there exists a S element signal in the cycled electrode, which comes from the S/C composite. This is also confirmed by the EDX elemental mapping images (Figure 4e−h) that S mainly stems from the dispersed carbon matrix in sharp contrast with other element distribution in the electrode. All of the above results reveal that the stable carbon framework with S confined in its micropores can maintain close contact with active particles to form a steady and continuous conductive network, which is beneficial for reducing the interfacial impedance and preserving good cycle stability of the cathode electrode.

Figure 5 shows a comprehensive comparison of various reported presodiation additives. Anode presodiation additives (such as Na_3P and Na powders) often display higher donable sodium-ion specific capacity than cathode presodiation additives, contributing to higher sodium compensation efficiency. However, these anode presodiation additives possess high chemical reactivity and often are very sensitive to moisture in ambient conditions. Thus, they are not compatible with the current regular electrode fabrication procedures. Cathode presodiation additives can be easily handled in the electrode and battery fabrication process due to their much better environmental stability than the anode presodiation additives and show promise for industrialization in the near future. Note that we performed the cathode fabrication with Na_2S/C nanocomposite using a regular slurry fabrication approach, showing the compatibility with the industrial electrode fabrication process. Therefore, the as-synthesized Na_2S/C presodiation additive meets the above-mentioned basic requirements, including no detrimental gas generation during the sodium donation process, and the highest specific capacity among the previously reported presodiation additives and potential compatibility with the current battery manufacturing.

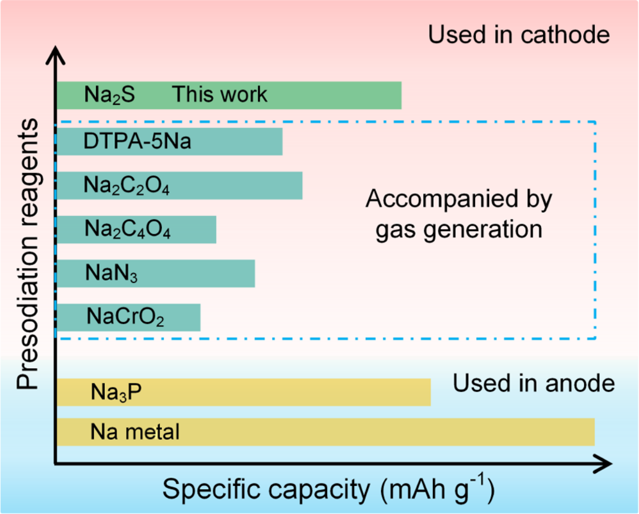

Figure 5. Comparison of different presodiation reagents for Na-ion batteries. Na_2S (this work), DTPA-5Na,[16] $Na_2C_2O_4$,[15] $Na_2C_4O_4$,[14] NaN_3,[17] and $NaCrO_2$[13] were used as cathode presodiation materials. Na_3P[49] and Na metal[11] were used as anode presodiation materials.

4. CONCLUSIONS

A well-designed Na_2S/C nanocomposite featuring ultrafine Na_2S nanoclusters confined in micropores of a highly conductive ZIF-8-derived N-doped carbon framework was developed as a high-efficiency presodiation reagent for SIBs to compensate for the initial sodium loss. The conductive carbon framework constrained polysulfide dissolution into the electrolyte and provided an electronic pathway for the insulating Na_2S and S. When used as a presodiation additive for the $Na_3V_2(PO_4)_3$-based cathode, higher initial charge specific capacity was achieved for the $Na_3V_2(PO_4)_3$ cathode with the addition of Na_2S/C nanocomposite, without negative effect on the capacity and cycling stability of the cathode. The supplied extra electrochemically active sodium can compensate for the sodium loss at the anode, leading to the improved energy density of the full cells. The results described here bring the research community a step closer to the achievement of high-energy-density SIBs.

■ ASSOCIATED CONTENT

Supporting Information

The Supporting Information is available free of charge at https://pubs.acs.org/doi/10.1021/acsami.1c05144.

Additional TEM, HAADF-STEM, and the corresponding elemental mapping images; additional XRD results; charge/discharge profiles and cycling performances for hard carbon anodes and full cells; Nyquist plots of the

NVPO electrodes at different cycles; and additional SEM images (PDF)

AUTHOR INFORMATION

Corresponding Author

Yongming Sun − *Wuhan National Laboratory for Optoelectronics, Huazhong University of Science and Technology, Wuhan 430074, China;* orcid.org/0000-0001-8528-525X; Email: yongmingsun@hust.edu.cn

Authors

Xiaoxiao Liu − *Wuhan National Laboratory for Optoelectronics, Huazhong University of Science and Technology, Wuhan 430074, China*

Yuchen Tan − *Wuhan National Laboratory for Optoelectronics, Huazhong University of Science and Technology, Wuhan 430074, China*

Wenyu Wang − *Wuhan National Laboratory for Optoelectronics, Huazhong University of Science and Technology, Wuhan 430074, China*

Peng Wei − *Wuhan National Laboratory for Optoelectronics, Huazhong University of Science and Technology, Wuhan 430074, China*

Zhi Wei Seh − *Institute of Materials Research and Engineering, Agency for Science, Technology and Research (A*STAR), Singapore 138634, Singapore;* orcid.org/0000-0003-0953-567X

Complete contact information is available at: https://pubs.acs.org/10.1021/acsami.1c05144

Author Contributions

X.L. and Y.S. conceived the idea and designed the experiments. Y.T., W.W., and P.W. assisted in the experimental work. X.L., Z.W.S., and Y.S. wrote the manuscript and all authors edited the manuscript.

Notes

The authors declare no competing financial interest.

ACKNOWLEDGMENTS

This work was supported by the National Natural Science Foundation of China (Grant Nos. 52002136, 52072137, and 51802105), the China Postdoctoral Science Foundation (Grant No. 2020T130216), and the Innovation Fund of Wuhan National Laboratory for Optoelectronics. The authors would also like to thank the Analytical and Testing Center of Huazhong University of Science and Technology (HUST) as well as the Center for Nanoscale Characterization & Devices of Wuhan National Laboratory for Optoelectronics (WNLO) for providing the facilities to conduct the characterizations. Z.W.S. acknowledges the support of the Singapore National Research Foundation (NRF-NRFF2017-04).

REFERENCES

(1) Vaalma, C.; Buchholz, D.; Weil, M.; Passerini, S. A Cost and Resource Analysis of Sodium-Ion Batteries. *Nat. Rev. Mater.* **2018**, *3*, No. 18013.

(2) Hwang, J.-Y.; Myung, S.-T.; Sun, Y.-K. Sodium-Ion Batteries: Present and Future. *Chem. Soc. Rev.* **2017**, *46*, 3529−3614.

(3) Wu, W.; Hou, S.; Zhang, C.; Zhang, L. A Dendrite-free Na-Na_2S-Carbon Hybrid toward a Highly Stable and Superior Sodium Metal Anode. *ACS Appl. Mater. Interfaces* **2020**, *12*, 27300−27306.

(4) Zhang, L.; Zhang, B.; Dou, Y.; Wang, Y.; Al-Mamun, M.; Hu, X.; Liu, H. Self-Assembling Hollow Carbon Nanobeads into Double-Shell Microspheres as a Hierarchical Sulfur Host for Sustainable Room-Temperature Sodium-Sulfur Batteries. *ACS Appl. Mater. Interfaces* **2018**, *10*, 20422−20428.

(5) Huang, Y.; Zheng, Y.; Li, X.; Adams, F.; Luo, W.; Huang, Y.; Hu, L. Electrode Materials of Sodium-Ion Batteries toward Practical Application. *ACS Energy Lett.* **2018**, *3*, 1604−1612.

(6) Ma, R.; Fan, L.; Chen, S.; Wei, Z.; Yang, Y.; Yang, H.; Qin, Y.; Lu, B. Offset Initial Sodium Loss To Improve Coulombic Efficiency and Stability of Sodium Dual-Ion Batteries. *ACS Appl. Mater. Interfaces* **2018**, *10*, 15751−15759.

(7) Liu, X.; Liu, T.; Wang, R.; Cai, Z.; Wang, W.; Yuan, Y.; Shahbazian-Yassar, R.; Li, X.; Wang, S.; Hu, E.; Yang, X.-Q.; Xiao, Y.; Amine, K.; Lu, J.; Sun, Y. Prelithiated Li-Enriched Gradient Interphase toward Practical High-Energy NMC−Silicon Full Cell. *ACS Energy Lett.* **2021**, *6*, 320−328.

(8) Liu, X. X.; Shu, T.; Zhang, L.; Li, F. Y.; Hu, X. L. Mo-Catalysis-Assisted Expeditious Synthesis of N-Doped Erythrocyte-like Hollow Porous Carbons for Sodium Storage. *Carbon* **2019**, *143*, 240−246.

(9) Zou, K. Y.; Deng, W. T.; Cai, P.; Deng, X. L.; Wang, B. W.; Liu, C.; Li, J. Y.; Hou, H. S.; Zou, G. Q.; Ji, X. B. Prelithiation/Presodiation Techniques for Advanced Electrochemical Energy Storage Systems: Concepts, Applications, and Perspectives. *Adv. Funct. Mater.* **2020**, No. 2005581.

(10) Moeez, I.; Jung, H. G.; Lim, H. D.; Chung, K. Y. Presodiation Strategies and Their Effect on Electrode-Electrolyte Interphases for High-Performance Electrodes for Sodium-Ion Batteries. *ACS Appl. Mater. Interfaces* **2019**, *11*, 41394−41401.

(11) Tang, J. L.; Kye, D. K.; Pol, V. G. Ultrasound-Assisted Synthesis of Sodium Powder as Electrode Additive to Improve Cycling Performance of Sodium-Ion Batteries. *J. Power Sources* **2018**, *396*, 476−482.

(12) Liu, X.; Tan, Y.; Liu, T.; Wang, W.; Li, C.; Lu, J.; Sun, Y. A Simple Electrode-Level Chemical Presodiation Route by Solution Spraying to Improve the Energy Density of Sodium-Ion Batteries. *Adv. Funct. Mater.* **2019**, *29*, No. 1903795.

(13) Shen, B.; Zhan, R.; Dai, C.; Li, Y.; Hu, L.; Niu, Y.; Jiang, J.; Wang, Q.; Xu, M. Manipulating Irreversible Phase Transition of $NaCrO_2$ towards An Effective Sodium Compensation Additive for Superior Sodium-Ion Full Cells. *J. Colloid Interface Sci.* **2019**, *553*, 524−529.

(14) Shanmukaraj, D.; Kretschmer, K.; Sahu, T.; Bao, W.; Rojo, T.; Wang, G.; Armand, M. Highly Efficient, Cost Effective, and Safe Sodiation Agent for High-Performance Sodium-Ion Batteries. *ChemSusChem* **2018**, *11*, 3286−3291.

(15) Niu, Y. B.; Guo, Y. J.; Yin, Y. X.; Zhang, S. Y.; Wang, T.; Wang, P.; Xin, S.; Guo, Y. G. High-Efficiency Cathode Sodium Compensation for Sodium-Ion Batteries. *Adv. Mater.* **2020**, No. e2001419.

(16) Jo, J. H.; Choi, J. U.; Park, Y. J.; Ko, J. K.; Yashiro, H.; Myung, S.-T. A New Pre-sodiation Additive for Sodium-Ion Batteries. *Energy Storage Mater.* **2020**, *32*, 281−289.

(17) Singh, G.; Acebedo, B.; Cabanas, M. C.; Shanmukaraj, D.; Armand, M.; Rojo, T. An Approach to Overcome First Cycle Irreversible Capacity in P2-$Na_{2/3}[Fe_{1/2}Mn_{1/2}]O_2$. *Electrochem. Commun.* **2013**, *37*, 61−63.

(18) Martinez De Ilarduya, J.; Otaegui, L.; López del Amo, J. M.; Armand, M.; Singh, G. NaN_3 Addition, A Strategy to Overcome the Problem of Sodium Deficiency in P2-$Na_{0.67}[Fe_{0.5}Mn_{0.5}]O_2$ Cathode for Sodium-Ion Battery. *J. Power Sources* **2017**, *337*, 197−203.

(19) Bloi, L. M.; Pampel, J.; Dörfler, S.; Althues, H.; Kaskel, S. Sodium Sulfide Cathodes Superseding Hard Carbon Pre-sodiation for the Production and Operation of Sodium−Sulfur Batteries at Room Temperature. *Adv. Energy Mater.* **2020**, *10*, No. 1903245.

(20) Yu, X.; Manthiram, A. Na_2S-Carbon Nanotube Fabric Electrodes for Room-Temperature Sodium-Sulfur Batteries. *Chem. - Eur. J.* **2015**, *21*, 4233−4237.

(21) Xu, J. L.; Chen, J. Z.; Zhou, S.; Han, C. P.; Xu, M. J.; Zhao, N.; Wong, C. P. Sequentially-Processed $Na_3V_2(PO_4)_3$ for Cathode

Material of Aprotic Sodium Ion Battery. *Nano Energy* **2018**, *50*, 323−330.

(22) Cao, X. X.; Pan, A. Q.; Yin, B.; Fang, G. Z.; Wang, Y. P.; Kong, X. Z.; Zhu, T.; Zhou, J.; Cao, G. Z.; Liang, S. Q. Nanoflake-Constructed Porous $Na_3V_2(PO_4)_3$/C Hierarchical Microspheres as a Bicontinuous Cathode for Sodium-Ion Batteries Applications. *Nano Energy* **2019**, *60*, 312−323.

(23) Chung, S. H.; Manthiram, A. Current Status and Future Prospects of Metal-Sulfur Batteries. *Adv. Mater.* **2019**, *31*, No. e1901125.

(24) Zhang, B. W.; Sheng, T.; Wang, Y. X.; Chou, S.; Davey, K.; Dou, S. X.; Qiao, S. Z. Long-Life Room-Temperature Sodium-Sulfur Batteries by Virtue of Transition-Metal-Nanocluster-Sulfur Interactions. *Angew. Chem., Int. Ed.* **2019**, *58*, 1484−1488.

(25) Kumar, V.; Eng, A. Y. S.; Wang, Y.; Nguyen, D.-T.; Ng, M.-F.; Seh, Z. W. An Artificial Metal-Alloy Interphase for High-Rate and Long-Life Sodium−Sulfur Batteries. *Energy Storage Mater.* **2020**, *29*, 1−8.

(26) Wang, C.; Wang, H.; Hu, X.; Matios, E.; Luo, J.; Zhang, Y.; Lu, X.; Li, W. Frogspawn-Coral-Like Hollow Sodium Sulfide Nanostructured Cathode for High-Rate Performance Sodium-Sulfur Batteries. *Adv. Energy Mater.* **2019**, *9*, No. 1803251.

(27) Wang, Y. X.; Zhang, B. W.; Lai, W. H.; Xu, Y. F.; Chou, S. L.; Liu, H. K.; Dou, S. X. Room-Temperature Sodium-Sulfur Batteries: A Comprehensive Review on Research Progress and Cell Chemistry. *Adv. Energy Mater.* **2017**, *7*, No. 1602829.

(28) Zheng, S.; Yi, F.; Li, Z.; Zhu, Y.; Xu, Y.; Luo, C.; Yang, J.; Wang, C. Copper-Stabilized Sulfur-Microporous Carbon Cathodes for Li-S Batteries. *Adv. Funct. Mater.* **2014**, *24*, 4156−4163.

(29) Fan, L.; Ma, R.; Yang, Y.; Chen, S.; Lu, B. Covalent Sulfur for Advanced Room Temperature Sodium-Sulfur Batteries. *Nano Energy* **2016**, *28*, 304−310.

(30) Aslam, M. K.; Seymour, I. D.; Katyal, N.; Li, S.; Yang, T.; Bao, S. J.; Henkelman, G.; Xu, M. Metal Chalcogenide Hollow Polar Bipyramid Prisms as Efficient Sulfur Hosts for Na-S Batteries. *Nat. Commun.* **2020**, *11*, No. 5242.

(31) Cravillon, J.; Nayuk, R.; Springer, S.; Feldhoff, A.; Huber, K.; Wiebcke, M. Controlling Zeolitic Imidazolate Framework Nano- and Microcrystal Formation: Insight into Crystal Growth by Time-Resolved in Situ Static Light Scattering. *Chem. Mater.* **2011**, *23*, 2130−2141.

(32) Li, Z.; Xiao, Z.; Wang, S.; Cheng, Z.; Li, P.; Wang, R. Engineered Interfusion of Hollow Nitrogen-Doped Carbon Nanospheres for Improving Electrochemical Behavior and Energy Density of Lithium−Sulfur Batteries. *Adv. Funct. Mater.* **2019**, *29*, No. 1902322.

(33) Song, J.; Xu, T.; Gordin, M. L.; Zhu, P.; Lv, D.; Jiang, Y.-B.; Chen, Y.; Duan, Y.; Wang, D. Nitrogen-Doped Mesoporous Carbon Promoted Chemical Adsorption of Sulfur and Fabrication of High-Areal-Capacity Sulfur Cathode with Exceptional Cycling Stability for Lithium-Sulfur Batteries. *Adv. Funct. Mater.* **2014**, *24*, 1243−1250.

(34) Li, N.; Yu, L.; Yang, J.; Zheng, B.; Qiu, X.; Xi, J. Identifying the Active Sites and Multifunctional Effects in Nitrogen-Doped Carbon Microtube Interlayer for Confining-Trapping-Catalyzing Polysulfides. *Nano Energy* **2021**, *79*, No. 105466.

(35) Zhang, B.; Qin, X.; Li, G. R.; Gao, X. P. Enhancement of Long Stability of Sulfur Cathode by Encapsulating Sulfur into Micropores of Carbon Spheres. *Energy Environ. Sci.* **2010**, *3*, 1531−1537.

(36) Li, Z.; Yuan, L. X.; Yi, Z. Q.; Sun, Y. M.; Liu, Y.; Jiang, Y.; Shen, Y.; Xin, Y.; Zhang, Z. L.; Huang, Y. H. Insight into the Electrode Mechanism in Lithium-Sulfur Batteries with Ordered Microporous Carbon Confined Sulfur as the Cathode. *Adv. Energy Mater.* **2014**, *4*, No. 1301473.

(37) Shen, Y.; Zhang, J.; Pu, Y.; Wang, H.; Wang, B.; Qian, J.; Cao, Y.; Zhong, F.; Ai, X.; Yang, H. An Effective Chemical Prelithiation Strategy for Building a Silicon/Sulfur Li-Ion Battery. *ACS Energy Lett.* **2019**, *4*, 1717−1724.

(38) Liu, X.; Tan, Y.; Wang, W.; Li, C.; Seh, Z. W.; Wang, L.; Sun, Y. Conformal Prelithiation Nanoshell on $LiCoO_2$ Enabling High-Energy Lithium-Ion Batteries. *Nano Lett.* **2020**, *20*, 4558−4565.

(39) Wu, Y.; Momma, T.; Ahn, S.; Yokoshima, T.; Nara, H.; Osaka, T. On-Site Chemical Pre-lithiation of S Cathode at Room Temperature on a 3D Nano-structured Current Collector. *J. Power Sources* **2017**, *366*, 65−71.

(40) Guo, B.; Du, W.; Yang, T.; Deng, J.; Liu, D.; Qi, Y.; Jiang, J.; Bao, S. J.; Xu, M. Nickel Hollow Spheres Concatenated by Nitrogen-Doped Carbon Fibers for Enhancing Electrochemical Kinetics of Sodium-Sulfur Batteries. *Adv. Sci.* **2020**, *7*, No. 1902617.

(41) Wang, N.; Wang, Y.; Bai, Z.; Fang, Z.; Zhang, X.; Xu, Z.; Ding, Y.; Xu, X.; Du, Y.; Dou, S.; Yu, G. High-Performance Room-Temperature Sodium−Sulfur Battery enabled by Electrocatalytic Sodium Polysulfides Full Conversion. *Energy Environ. Sci.* **2020**, *13*, 562−570.

(42) Tanibata, N.; Deguchi, M.; Hayashi, A.; Tatsumisago, M. All-Solid-State Na/S Batteries with a Na_3PS_4 Electrolyte Operating at Room Temperature. *Chem. Mater.* **2017**, *29*, 5232−5238.

(43) Yu, X.; Manthiram, A. Highly Reversible Room-Temperature Sulfur/Long-Chain Sodium Polysulfide Batteries. *J. Phys. Chem. Lett.* **2014**, *5*, 1943−1947.

(44) Yang, Z.; Chen, T.; Wu, C.; Qu, J.; Wu, Z.; Guo, X.; Zhong, B.; Liu, H.; Dou, S. Interpreting Abnormal Charge-Discharge Plateau Migration in Cu_xS during Long-Term Cycling. *ACS Appl. Mater. Interfaces* **2019**, *11*, 3961−3970.

(45) Guo, Q.; Li, S.; Liu, X.; Lu, H.; Chang, X.; Zhang, H.; Zhu, X.; Xia, Q.; Yan, C.; Xia, H. Ultrastable Sodium-Sulfur Batteries without Polysulfides Formation Using Slit Ultramicropore Carbon Carrier. *Adv. Sci.* **2020**, *7*, No. 1903246.

(46) Pan, X. X.; Chojnacka, A.; Jezowski, P.; Beguin, F. Na_2S Sacrificial Cathodic Material for High Performance Sodium-Ion Capacitors. *Electrochim. Acta.* **2019**, *318*, 471−478.

(47) Susanto, D.; Cho, M. K.; Ali, G.; Kim, J. Y.; Chang, H. J.; Kim, H. S.; Nam, K. W.; Chung, K. Y. Anionic Redox Activity as a Key Factor in the Performance Degradation of $NaFeO_2$ Cathodes for Sodium Ion Batteries. *Chem. Mater.* **2019**, *31*, 3644−3651.

(48) Zhu, Q. Z.; Zhao, Q.; An, Y. B.; Anasori, B.; Wang, H. R.; Xu, B. Ultra-Microporous Carbons Encapsulate Small Sulfur Molecules for High Performance Lithium-Sulfur Battery. *Nano Energy* **2017**, *33*, 402−409.

(49) Zhang, B.; Dugas, R.; Rousse, G.; Rozier, P.; Abakumov, A. M.; Tarascon, J. M. Insertion Compounds and Composites Made by Ball Milling for Advanced Sodium-Ion Batteries. *Nat. Commun.* **2016**, *7*, No. 10308.